Journal of Applied Polymer Science

Dynamic Properties of Magnetorheological Elastomers Based on Iron Sand and Natural Rubber

S. Raa Khimi,[1] K. L. Pickering,[1] B. R. Mace[2]
[1]School of Engineering, University of Waikato, Hamilton 3216, New Zealand
[2]Department of Mechanical Engineering, University of Auckland, Auckland 1142, New Zealand
Correspondence to: S. Raa Khimi (E-mail: klp@waikato.ac.nz)

ABSTRACT: In this study, magnetorheological elastomers (MREs) based on iron sand and natural rubber were prepared. The Taguchi method was employed to investigate the effect of a number of factors, namely, the iron sand content, iron sand particle size, and applied magnetic field during curing on the loss tangent (tan δ) and energy dissipated during cyclic loading. Tan δ was measured through dynamic mechanical analysis over a range of frequency (0.01–130 Hz), strain amplitude (0.1–4.5%), and temperature (-100 to 50°C). The energy dissipated was measured with a universal tester under cyclic tensile loading. The data were then statistically analyzed to predict the optimal combination of factors, and finally, experiments were conducted for verification. It was found that the iron sand content had the greatest influence on tan δ when measured over a range of frequency, and the energy dissipated during hysteresis tests. However, none of the factors showed a significant influence on tan δ when measured over a range of strain amplitude. Furthermore, the iron sand content and magnetic field were also found to influence the width of the peak in tan δ as a function of the temperature. The morphological characteristics of the MREs were also examined with scanning electron microscopy. © 2014 Wiley Periodicals, Inc. J. Appl. Polym. Sci. **2015**, *132*, 41506.

KEYWORDS: dynamic properties; magnetorheological elastomers; statistical methods

Received 28 April 2014; accepted 5 September 2014
DOI: 10.1002/app.41506

INTRODUCTION

A material with a high damping capability is desired from the viewpoint of vibration suppression in structures. Rubber is by far the most commonly used material for damping; here, damping relies on the energy absorbed due to viscous flow that occurs during deformation in this viscoelastic material. However, the enhancement of damping through rubber modification or rubber selection to increase the viscous flow, not surprisingly, generally results in a reduction in stiffness and strength.[1] More recently, magnetorheological elastomers (MREs) have been developed such that the inclusion of magnetic particles in rubber enables additional damping through magnetic interactions between neighbouring magnetic particles and interfacial damping between the particles and the rubber matrix. Furthermore, the damping and stiffness can be varied by the application of an applied magnetic field during fabrication or in service. MREs are often referred to as solid analogs of the previously developed magnetorheological fluids (MRFs) used in the damping of automotive suspensions. In MRFs, magnetic particles are contained within an oil. The main advantage of MREs over MRFs is that particle sedimentation is overcome. Moreover, MREs do not need containers or seals to hold the fluid or prevent leakage.[2] MREs can be used for damping, either alone or within a composite structures, such as those including steel plates.

MREs can be fabricated to contain a uniform suspension of magnetic particles (isotropic MREs). However, it has been found that when a magnetic field is applied during curing, chainlike structures of magnetic particles are formed within the rubber (which become anisotropic MREs); this provides much larger damping and stiffness values.[3] Figure 1 shows the structure of isotropic and anisotropic MREs. The formation of such chainlike structures relies on a mechanism such that when individual particles are exposed to an applied magnetic field, magnetic dipole moments pointing along the field direction are induced within them. A magnetic force will cause the north pole of one particle to attract the south pole of its neighbour; this results in the formation of chains and columnar structures inside the matrix. When the matrix is cured, the particle structure is set in place.[4]

The magnetic particles of choice for MREs are iron particles, and suitable matrix materials include natural rubber, silicone rubber, polybutadiene, polyisobutylene, polyisoprene, and polyurethene rubber.[3,5–10] These materials are nonmagnetic

© 2014 Wiley Periodicals, Inc.

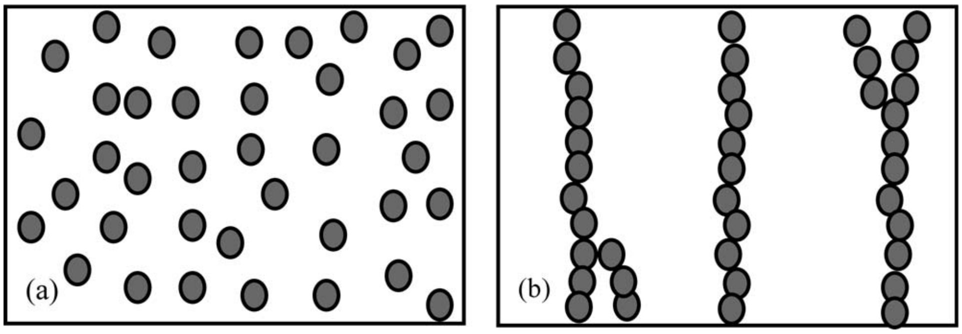

Figure 1. MRE structure: (a) isotropic and (b) anisotropic MRE.

viscoelastic materials into which the magnetic particles can be added and subsequently processed into a final solid form through conventional rubber or plastic processing.[11–13] Recent work has focused on carbonyl iron and natural rubber MRE because of their associated ease of processing and good damping performance.[14–16] However, one of the biggest challenges in the development of MREs is cost. Carbonyl iron particles, the most commonly used particles, are expensive at $13–15/kg in bulk. The more cheaply produced iron particles iron oxide (Fe_3O_4) and barium ferrite ($BaFe_{12}O_{19}$) tend to be irregular in shape, tend to have wider size distributions, and simply do not perform as well.[17,18] Some iron alloy particles actually perform better than carbonyl iron, but they are significantly more expensive.[19] It is apparent that more applications would quickly become commercially viable if the material cost could be reduced.

This work aims to fabricate iron sand and natural rubber MREs. Iron sand was chosen because it has a high permeability and saturation magnetization, has a low cost, and is readily available in New Zealand. It is derived from the erosion of andesitic and rhyolitic volcanic rocks, which are the main types of iron ore deposits in New Zealand. Iron sand is a dark, high-density sand that occurs along the west coast of the North Island from Wanganui to Kaipara Harbour near Auckland over a distance of 480 km. It contains titanomagnetite, a mineral itself containing iron and titanium, which is highly magnetic.[20,21]

The conventional approach of experimental design is that one factor is varied and the remaining factors are kept constant; it is expensive and time-consuming. Hence, several design-of-experiment methods have been developed that can reduce the number of experiments, time, and cost required to model the response functions.[22] Among them, the Taguchi method has had great success in the design and optimization of the controllable factors to achieve a high-quality product or process.[23,24] This method has been used successfully, for example, to optimize the processing conditions and chemical formulation in rubber.[25,26] As far we are aware, there has been no published analysis of the factors effecting the dynamic properties of MREs with the Taguchi method. In this study, the loss tangent (tan δ) was considered as the fundamental parameter to assess damping. Tan δ gives a comparison of the energy lost to that stored; it is obtained by dividing the loss modulus (G'') by the storage modulus (G').[1] However, another estimate of damping used in the literature is the amount of energy dissipated during cyclic deformation; this can be calculated from the area of the hysteresis loop. In the next section, the Taguchi method is briefly reviewed. Then, the experimental methods used to fabricate the MREs, the factors investigated, and the characterization methods are described. This is followed by a presentation of the results and discussion. Finally, the conclusions are summarized, and some finding remarks are made.

TAGUCHI METHOD

The Taguchi method, pioneered by Genichi Taguchi, provides a simple, efficient, and systematic approach to study the effects of multiple variables by identifying the performance trend for each factor and determining the combination that yields the optimum conditions.

The Taguchi method generally includes the following steps:

1. Identification of the factors and their levels.
2. Selection of an appropriate orthogonal array (OA) and assignment of the factors and levels to the OA.
3. The conducting of the experiment.
4. Analysis of the experimental data and determination of the optimal levels.
5. Verification of the optimum design factors through experimentation.

The key component in the design of the experiment is the identification of factors and their levels. With the finalized factors and levels, the Taguchi method makes use of an OA for experimental design. The Taguchi method allows for 18 different standards of OAs, and the details of OA selection are published in refs.[24,27] After OA selection, the experiments are carried out, and the results can then be analyzed with the signal-to-noise (S/N) ratio to determine the effect of each factor and the level that maximizes the performance. The S/N can be divided into three categories depending on the desired output performance: nominal (used where a target value is desired), the smaller the better, and the larger the better, for which eqs. (1), (2), and (3) are used, respectively, to determine S/N:

$$\frac{S}{N}=-10\log\frac{\sum_{i=0}^{n}(Y_i-\mathrm{D})^2}{n} \tag{1}$$

$$\frac{S}{N}=-10\log\frac{\sum_{i=0}^{n}Y_\mathrm{i}^2}{n} \tag{2}$$

$$\frac{S}{N} = -10\log\frac{\sum_{i=0}^{n}\left(\frac{1}{Y_i^2}\right)}{n} \tag{3}$$

where D is the average of the observed data, n is the number of observations, i is the level, and Y_i is the observed data at level i. Another function of S/N is that it is able to determine the ranking of factors through the calculation of the average effect of a factor at a level. This is given by simple statistical calculation as follows:[25]

$$Aj = \frac{\sum_{i=0}^{n}\left(\frac{S}{N}\right)i}{n} \tag{4}$$

where A_j is the average for factor j, $(S/N)_i$ represents the S/N observation of a factor at level i, and n represents the total number of observations for that factor. By plotting the average factor effect against the corresponding factor level, a main effect plot is obtained, and the trend of the influence of each factor on the results is extracted. The relative effects of factors affecting the response can be calculated by an analysis of variance (ANOVA). ANOVA is a powerful statistical analysis tool that can be used in the Taguchi method to determine statistically significant factors and to explore the relative contribution of each factor and level to the total variation. ANOVA provides information on the sum of squares (SS), degrees of freedom, percentage confidence level, and percentage contribution. SS is a measure of the total variability of the observed data. The SS is defined as follows:

$$\mathrm{SS} = \frac{\sum_{i=0}^{n} X_a^2}{n} - \frac{T^2}{N} \tag{5}$$

where a is the factor, X_a is the sum of the observed data at factor a, $T = \Sigma X_a$ is the sum of all of the data, and N is the total number of data points. The degrees of freedom represent the number of levels for each factor, which may vary independently and is equal to the number of levels of each factor minus one. The percentage confidence level represents the probability of the occurrence and the reliability of the data. The percentage contribution is calculated as follows:

$$\text{Percentage contribution} = \frac{SS_a}{SS_T} \times 100\% \tag{6}$$

where SS_a is the sum of squares of factor a and SS_T is the total sum of squares. With S/N and ANOVA analyzed, the optimal combination of the factors can be predicted, and finally, an experiment can be conducted to verify the optimal factors.

EXPERIMENTAL

Materials

A fixed masterbatch formulation for rubber was used in this study (Table I). Natural rubber (Standard Malaysian Rubber (SMR) L grade) and other chemicals, including zinc oxide, stearic acid, n-cyclohexyl-2-benzothiazole sulfenamide (CBS), tetramethylthiuram disulfide (TMTD), paraffin oil, and naphthenic oil, were all purchased from Field Rubber, Ltd. (Auckland). Iron sand was collected from Ngarunui Beach, Raglan. The iron sand was then milled with a planetary monomill (Pulverisette 6) produced by Fristech GmbH and subsequently sieved to obtain a wide range of particle size fractions.

Table I. Masterbatch Formulation

Material	Function	phr
Natural rubber	Raw material and matrix	100
ZnO	Activator/peptiser	5
Stearic acid	Activator/peptiser	1
CBS	Accelerator	2
TMTD	Accelerator	1
Paraffin oil	Plasticizer	2
Naphthenic oil	Plasticizer	3
Sulfur	Crosslinking agent	1.5

Experimental Design

Selection of Factors and Levels. In this study, three factors were considered: the iron sand content, particle size, and applied magnetic field during curing. These factors were varied at five levels, as shown in Table II, on the basis of the existing literature.[3,4,9,14,16]

Selection of OA and Analysis of Data. Given the three factors and five levels considered in this study, an L25 OA was selected for the Taguchi method. The L25 OA is shown in Table III and consisted of 25 experiments corresponding to 25 rows and three design factors assigned to the respective columns along with their levels. The analysis of the S/N was subsequently used to evaluate the experimental results. In this study, because the tan δ and amount of energy dissipated (hysteresis tests) were intended to be maximized, the larger-the-better target for S/N was chosen. ANOVA was used to statistically assess the percentage contribution and relationship between each factor. ANOVA was performed with STATISTICA software.

Preparation of the Iron Sand–Natural Rubber MREs. Formulations were determined according to the OA and were compounded with a conventional laboratory two-roll mill (model XK150) according to ASTM D 3184-80. The *nip gap* (the distance between the front and back rollers), time of compounding, and sequence of addition of the ingredients (rubber, activator, plasticizer, filler, accelerator, and crosslinking agent)

Table II. Experimental Control Factors and Their Respective Levels

Factor	Symbol	Unit	Level 1	Level 2	Level 3	Level 4	Level 5
Iron sand content	I	phr	0	30	50	70	100
Particle size	P	μm	0–32	32–45	45–56	56–75	75–106
Magnetic field	M	mT	0	300	500	700	1000

Table III. Experimental Layout of an L25 OA According to the Taguchi Method

	Factors and their levels		
Sample type	*I*	*P*	*M*
1	1	1	1
2	1	2	2
3	1	3	3
4	1	4	4
5	1	5	5
6	2	1	2
7	2	2	3
8	2	3	4
9	2	4	5
10	2	5	1
11	3	1	3
12	3	2	4
13	3	3	5
14	3	4	1
15	3	5	2
16	4	1	4
17	4	2	5
18	4	3	1
19	4	4	2
20	4	5	3
21	5	1	5
22	5	2	1
23	5	3	2
24	5	4	3
25	5	5	4

were kept constant for all of the compounds. The cure time at 150°C was then determined according to the procedure, as described in ref. 28. Compounded rubber samples weighing 13 g were placed in a 60 × 50 × 3 mm mold. The isotropic MREs were cured in a compression moulder at 150°C under a pressure of approximately 12 MPa. The anisotropic MREs were subjected to an external magnetic field in a specially developed electromagnetic thermally coupled device (as shown in Figure 2) at 80°C for 30 min and were subsequently cured in a compression moulder at 150°C under a pressure of approximately 12 MPa. Finally, postcure treatment was performed by the cooling of the anisotropic MREs at room temperature for 30 min under an external magnetic field of the same strength as that used during precuring. The postcure treatment was necessary to reorientate the magnetic dipoles after they were exposed to the compression stress during compression molding.

Characterization

Dynamic Mechanical Analysis (DMA). DMA was carried out with a PerkinElmer dynamic mechanical analyzer (DMA 8000). Tan δ was measured over a wide range of frequency, strain amplitude, and temperature. The influence of the frequency and strain amplitude on tan δ was assessed with two circular disc specimens with a diameter of 10 mm and a thickness of 3 mm in shear mode at room temperature. Tan δ was measured over the frequency range 0.01–130 Hz at a fixed strain amplitude of 0.5% and over the strain amplitude range 0.1–4.5% at a fixed frequency of 100 Hz. To determine the influence of the temperature on tan δ, the samples were analyzed in dual-cantilever mode at a frequency of 1 Hz with a strain amplitude of 0.5% and over the temperature range from −100 to 50°C. The samples were then heated at rate of 2°C/min. The samples were rectangular with dimensions of 30 ×6 ×3 mm^3.

Hysteresis. *Hysteresis loss* is defined as the amount of energy dissipated during cyclic deformation when the samples are stretched and then allowed to retract at the same rate to their unstretched state. In this study, the hysteresis loss was determined on tensile dumbbells with an Instron 4204 at a crosshead speed of 500 mm/min according to ASTM D 412-80. The stress–strain curve was recorded, and the hysteresis loss was calculated as follows:

Hysteresis loss = Area under the loading curve − Area under the recovery curve (7)

Morphology. The microstructures of the isotropic and anisotropic MREs were observed with scanning electron microscopy (SEM; Hitachi S-4700). The samples were cut into pieces with a surface area of 5 × 3 mm^2 and coated with a thin layer of platinum before observation at an accelerating voltage of 20 kV.

RESULTS AND DISCUSSION

The trends obtained in this study were similar to typical trends observed in previous works for the influence of frequency,[14,29,30] strain amplitude,[16,31] and temperature[32,33] on tan δ and the hysteresis loop obtained after a complete reversed stress cycle.[34,35] To calculate the optimum levels for the different factors with *S/N* and ANOVA, reference points for tan δ were selected. To optimize tan δ over a range of frequency from 0.01 to 130 Hz, the maximum value of tan δ was taken as the reference point; it was consistently observed at 130 Hz (the maximum frequency applied). To optimize tan δ over a range of strain amplitude (0.1–4.5%), the reference point was chosen to be within the plateau region at 3% strain amplitude. With respect to the choice of a reference point over a range of temperature, attention was given to the peak of the curve of tan δ versus temperature, which represented the glass-transition temperature (T_g), where the material undergoes drastic changes in the mechanical energy of the molecular vibrational motion. The addition of particulate

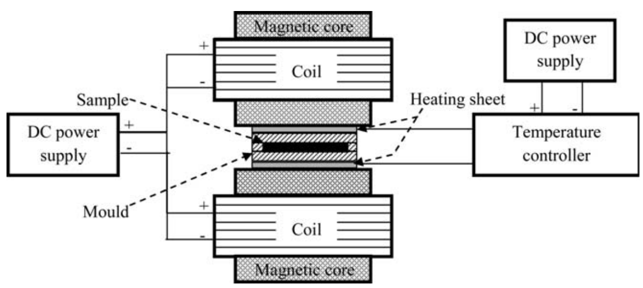

Figure 2. Sketch of the specially developed electromagnetic, heat-coupled device (DC = direct current).

Table IV. Tan δ and Hysteresis Loss Used to the Calculate *S*/*N*s and ANOVA

Sample type	Maximum tan δ over 0.01–130 Hz (130 Hz)[a]	Tan δ at a plateau over 0.1–4.5% strain amplitude (3%)[b]	Tan δ in the transition region of −47 to 0°C (−35°C)[c]	Hysteresis loss (kJ/m^3)
1	0.093	0.098	0.758	31.59
2	0.093	0.098	0.749	31.96
3	0.097	0.099	0.720	31.71
4	0.096	0.098	0.758	31.72
5	0.095	0.098	0.744	32.44
6	0.111	0.103	1.082	39.04
7	0.078	0.129	0.870	52.46
8	0.131	0.112	0.946	69.98
9	0.095	0.137	1.142	55.11
10	0.112	0.113	0.958	49.46
11	0.118	0.099	0.881	45.55
12	0.114	0.107	1.025	94.15
13	0.125	0.110	1.128	110.92
14	0.103	0.090	0.676	96.41
15	**0.171**	**0.155**	0.670	57.10
16	0.133	0.104	0.913	57.58
17	0.112	0.098	**1.216**	119.48
18	0.158	0.118	0.843	95.26
19	0.161	0.134	0.952	70.09
20	0.169	0.130	0.842	75.51
21	0.114	0.095	1.061	100.05
22	0.113	0.098	0.920	99.29
23	0.103	0.090	0.851	**154.61**
24	0.151	0.148	0.851	104.10
25	0.078	0.071	0.946	133.34

The highest values are shown in bold.
[a] Strain amplitude = 0.5%.
[b] Frequency = 100 Hz.
[c] Strain amplitude = 0.5% and frequency = 1 Hz.

fillers into rubber is generally not expected to change the temperature at which tan δ reaches a peak. What is commonly apparent, however, is a broadening of the transition region after T_g to the plateau region.[32,36] In this study, T_g of the natural rubber was −47°C, and the transition region after T_g to the plateau region was observed at −47 to 0°C. To reflect the broadening of the peak, a reference point for tan δ was selected at −35°C. In hysteresis testing, the amount of energy dissipated was calculated from the area of the hysteresis loop. Table IV shows the values of the tan δ and hysteresis loss obtained for these reference points, which were subsequently used to calculate the *S*/*N*s and ANOVA, with each value representing an average from the three samples. The highest values for each test type are shown in bold.

Morphology

Figure 3 shows SEM images of the isotopic and anisotropic MREs. From the SEM micrographs, it can be seen that the isotropic MREs had a homogeneous iron sand particle distribution in the rubber matrix without obvious aggregation [Figure 3(a)]. Figure 3(b–e) shows anisotropic MREs cured at different magnetic fields. Clearly, as expected, the application of a magnetic field at elevated temperature allowed the iron sand particles to organize into chainlike columnar structures. It can also be noted that the chains became longer and more aligned as the magnetic field strength increased. A higher magnification micrograph [Figure 3(f)] highlighted that there were obvious gaps between the iron sand particles and rubber; this suggested weak interaction between the iron sand and rubber.

Effect of the Frequency on Tan δ

The trends for the influence of the frequency on tan δ when the factors were varied over their different levels are shown on the main effect plots in Figure 4. As discussed earlier, the higher the value of *S*/*N* was, the better the signal was; this implied that the highest value in the main effect plots could be used as the conditions to attain the optimized tan δ. The *S*/*N* increased with increasing iron sand content until it reached a maximum value at 70 parts per hundred rubber (phr) and, thereafter, decreased at the highest iron sand content (100

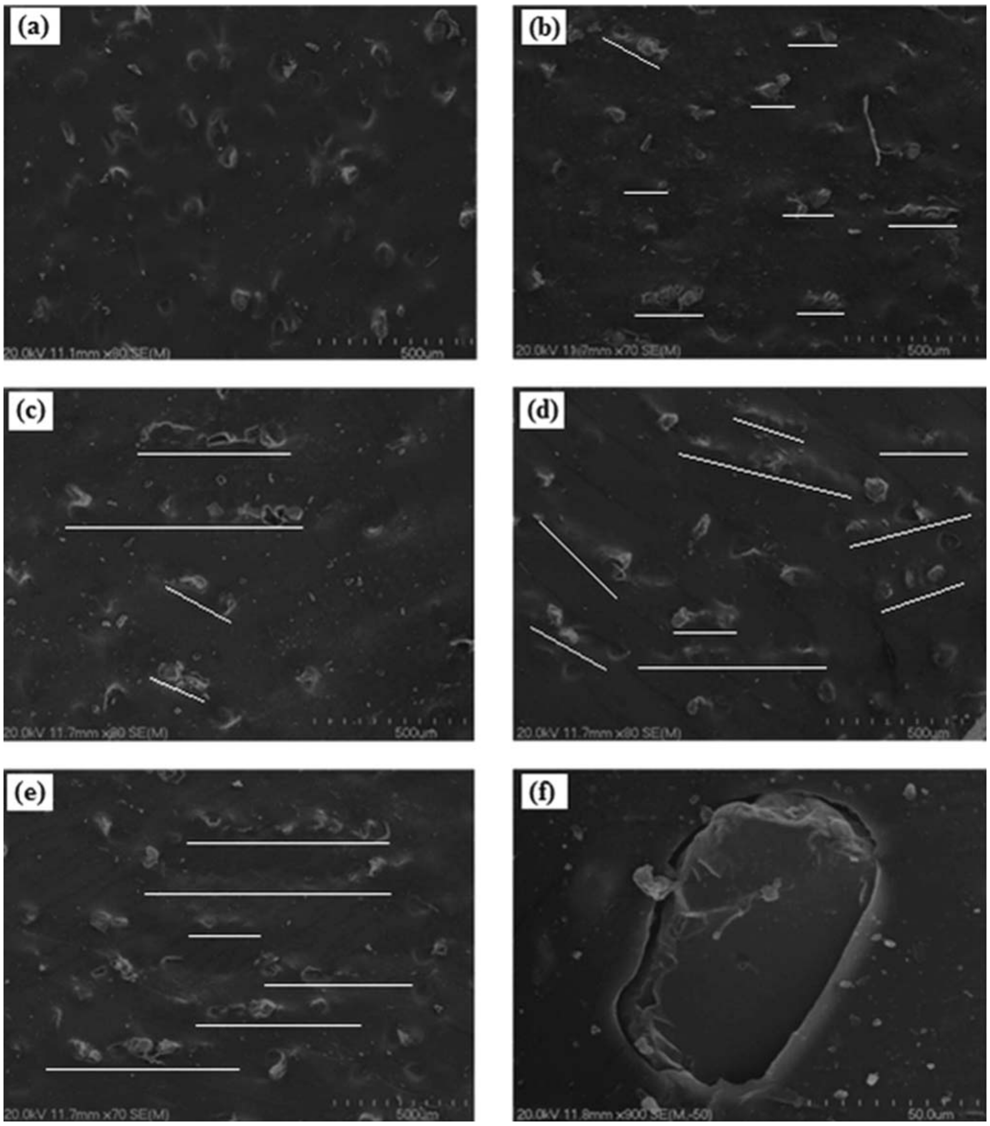

Figure 3. SEM images of the iron sand–natural rubber MREs: (a) isotropic MRE, 0 mT; (b) anisotropic MRE, 300 mT; (c) anisotropic MRE, 500 mT; (d) anisotropic MRE, 700 mT; (e) anisotropic MRE, 1000mT; and (f) interphase of the iron sand–natural rubber matrix.

phr). The increase of S/N with increasing iron sand content could be explained by the increase in energy absorbed due to interfacial friction caused by the increase in the interfacial area with the increase in iron sand content. The decrease in S/N at the highest iron sand content could be explained by the poor dispersion of iron sand particles, which was due to the insufficient amounts of rubber matrix to wet the iron sand thoroughly. Similar findings were observed in other studies.[15,37] As shown in Figures 4(b,c), the particle size and magnetic field had minimal influence on S/N, but the S/Ns at 45–56 μm and 300 mT were the highest. The minimal influence of the magnetic field on the S/Ns appeared to be due to the minimal increase of particle separation as the test was performed at a low fixed strain amplitude (0.5%) in shear mode such that particle chains generally rotated rather than extended. The results suggest that the highest value for tan δ might have been obtained with 70-phr iron sand, a 45–56-μm particle size, and a 300-mT magnetic field during curing.

Table V shows the ANOVA results for the effect of the frequency on tan δ. It can be seen from the level of contribution that the iron sand content had the greatest influence on tan δ, with a 99.9% confidence level. The particle size and magnetic field showed much less influence (lower percentage contribution), with confidence levels of 99 and 97%, respectively.

The final and essential step to complete the Taguchi analysis, namely, the conducting of an experiment to verify the suggested optimum conditions, was carried out with the optimized conditions (70-phr iron sand, 45–56-μm particle size, and 300-mT magnetic field), and the value of tan δ found (0.22) was indeed higher than the highest value achieved previously (0.171 for sample type 15). This supported the optimum conditions suggested by S/N and ANOVA. The variation of tan δ with frequency is shown in Figure 5(a). Tan δ was higher for the optimized sample over the whole frequency range explored. G' and G'' are also plotted in Figure 5(b,c) to help highlight the mechanisms involved. G' and G'', similar to tan δ, were

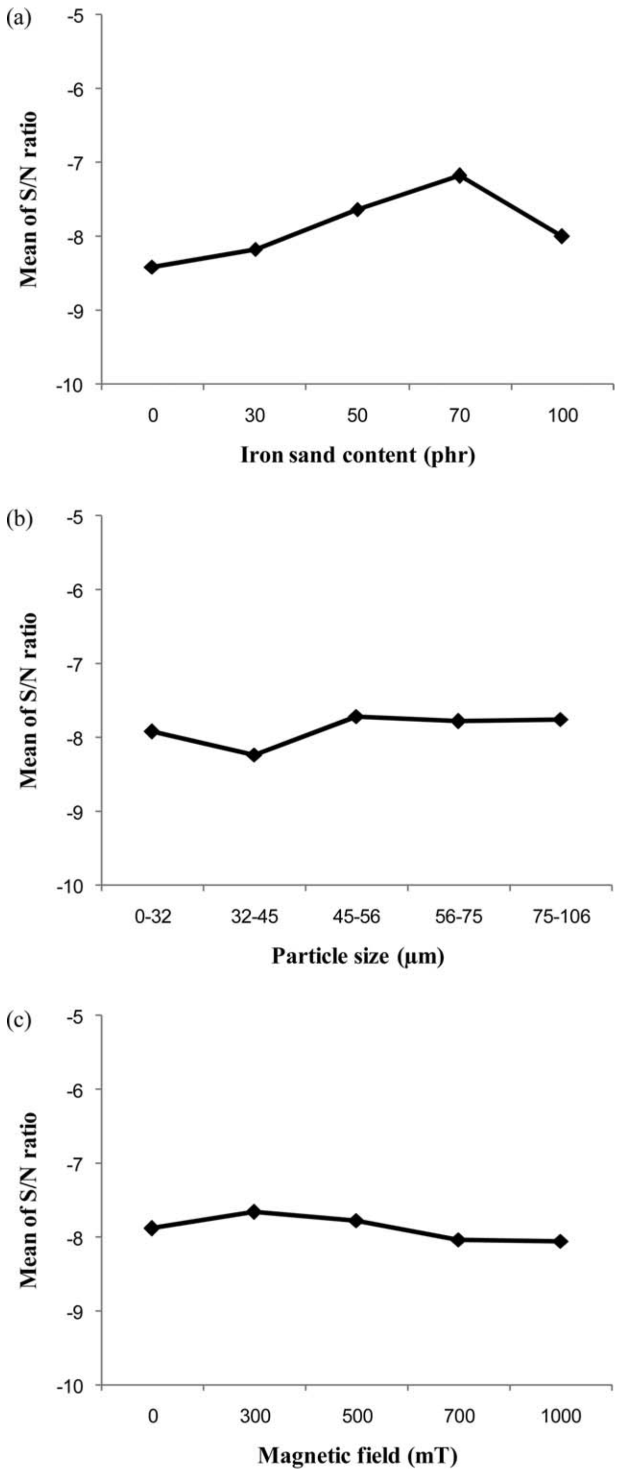

Figure 4. Main effect plots for the *S*/*N* of tan δ at 130 Hz: (a) effect of the iron sand content, (b) effect of the iron sand particle size, and (c) effect of the magnetic field during curing.

frequency-dependent, and the increase in tan δ as the frequency increased was mainly due to the increase in G'' as opposed to G'. The increase in G'' could again be explained by the increased energy loss due to the increase of interfacial friction between the iron sand and rubber with increasing frequency.

Effect of the Strain Amplitude on Tan δ

Figure 6 shows the main effect plots of the *S*/*N*s for the influence of strain amplitude on tan δ. The highest *S*/*N*s were observed at a 30-phr iron sand content, a 56–75-μm particle size, and a 500-mT magnetic field during curing. However, no obvious trend of the *S*/*N*s was observed for any factor as the level changed. This was attributed to the poor bonding between the iron sand and rubber, as supported by their morphology. This was in agreement with results reported by other researchers.[37] The weak interaction between the iron sand and natural rubber was fully disrupted at low strain amplitudes, and therefore, at high strain amplitudes, the damping was dominated by the viscous flow of the rubber matrix. As was the case for the selected reference point (3% strain amplitude) here, it should also be noted that the suggested optimum conditions were different compared with the optimum conditions for the effect of the frequency on tan δ (70 phr, 45–56 μm, and 300 mT). A lower optimum iron sand content (30 phr) supported that at the reference point for the experiment on the effect of the strain amplitude on tan δ, the energy absorbed was more dominated by the viscous flow in the rubber matrix. However, the suggested optimum magnetic field was higher; this indicated that the formation of longer particle chains opposed the higher shearing force with increasing strain amplitudes, such that the particle chain orientation changed and transformed elastic energy into magnetic energy, which then dissipated by magnetic hysteresis.[6,38]

Table VI shows the ANOVA results for the effect of the strain amplitude on tan δ. The variability for each factor was tested at a 99.9% confidence level. None of the factors had a significant influence on tan δ, and hence, the percentage contribution was approximately the same for each factor.

As expected, an experiment with optimized conditions (30-phr iron sand content, 56–75-μm particle size, and 500-mT magnetic field) resulted in a slightly higher value of tan δ (0.160) compared with the highest achieved previously (0.155 for sample type 15). Figure 7 shows the tan δ, G', and G'' of the optimized sample and sample type 15 over a range of strain amplitude (0.1–4.5%). It was found that tan δ and G' were amplitude-dependent at low strain amplitudes and reached a plateau at about 1% strain amplitude. The amplitude dependence at low strain is typically attributed to the Payne effect.[39] This effect is frequently explained by the breakdown of filler aggregates to release trapped rubber to allow more viscous flow, the separation of dipole–dipole interaction between neighbouring particles, and filler–rubber detachment and reformation that increases with increasing strain amplitude. Once the strain amplitude is high enough, all of the interactions are destroyed to such an extent that it cannot be reconstructed, and the Payne effect diminishes. Consequently, the energy loss is largely reliant on the rubber matrix.

Effect of the Temperature on Tan δ

The main effect plots of the *S*/*N*s for the influence of the temperature on tan δ are depicted in Figure 8. The Taguchi method suggested that an optimized value for tan δ could be obtained with a 30-phr iron sand content, a 32–45-μm particle size, and

Table V. ANOVA Results for the Effect of the Frequency on Tan δ

Factor	SS	Degrees of freedom	Confidence level (%)	Contribution (%)
Iron sand content (phr)	0.024	4	99.9	72.73
Particle size (μm)	0.005	4	99	15.15
Magnetic field (mT)	0.004	4	97	12.12

a 1000-mT magnetic field during curing. As shown in Figure 8(a), *S*/*N*s of the filled compounds were higher compared to those of the unfilled compound. The addition of iron sand constrained the rubber chains and, therefore, increased the temper-

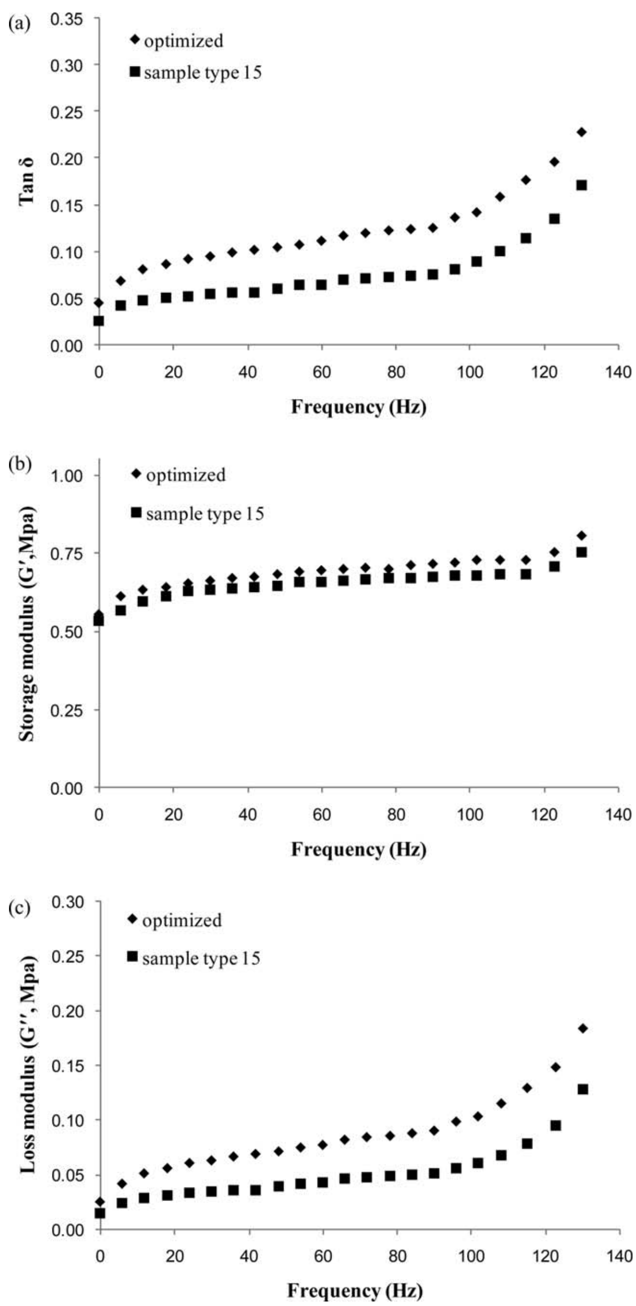

Figure 5. (a) Tan δ, (b) G', and (c) G'' versus the frequency for the optimized sample and sample type 15.

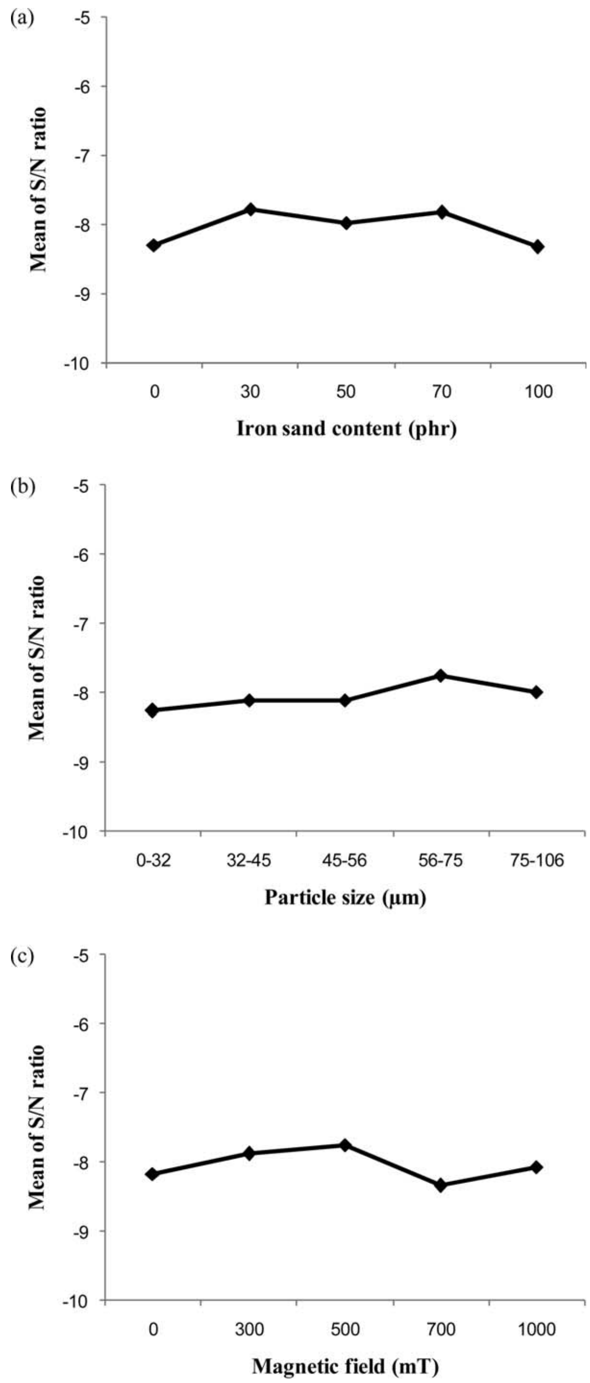

Figure 6. Main effect plots for *S*/*N* of tan δ at 3% strain amplitude: (a) effect of the iron sand content, (b) effect of the iron sand particle size, and (c) effect of the magnetic field during curing.

Table VI. ANOVA Results for the Effects of Tan δ on the Strain Amplitude

Factor	SS	Degrees of freedom	Confidence level (%)	Contribution (%)
Iron sand content (phr)	0.005	4	99.9	35.71
Particle size (μm)	0.004	4	99.9	28.57
Magnetic field (mT)	0.005	4	99.9	35.71

ature required for their mobility; this increased the relaxation at the reference temperature.[36] As shown in Figure 8(b), the *S/N*s decreased with increasing particle size; this was likely to be due to the decrease in the surface area of the iron sand adhered to the rubber. As shown in Figure 8(c), the *S/N* increased with increasing magnetic field until it reached a maximum at 1000 mT. This indicated that the formation of magnetic particle chains and columnar structures provided additional damping by further restriction of the intermolecular conformational changes during relaxation, as supported by the morphology. As also noted, the suggested optimum conditions were different compared with those observed previously for the effect of the frequency and strain amplitude on tan δ. As this test was performed in dual-cantilever mode at a fixed low frequency (1 Hz) and strain amplitude (0.5%) over the temperature range, the deformation of the material was much lower compared with that tested in shear loading. Therefore, at the selected reference point used for this experiment, the additional damping through interfacial friction and magnetic particle interaction was expected to be much lower. A lower optimum iron sand content (30 phr) supported that the damping was largely reliant on the intermolecular relaxation of the rubber matrix. However, the suggested optimum magnetic field at 1000 mT suggested that the energy absorbed by the formation of longer particle chains was not due to the separation of dipole–dipole interactions; perhaps the longer particle chains provided additional damping through further restriction of the intermolecular conformational changes during relaxation.

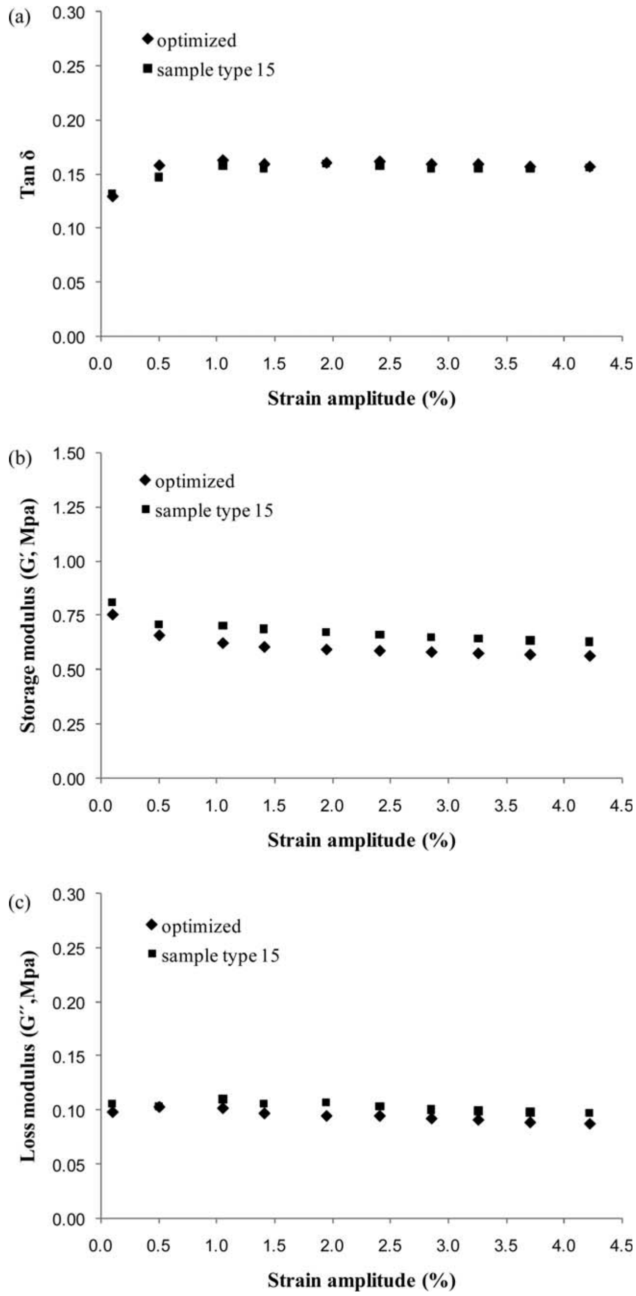

Figure 7. (a) Tan δ, (b) G', and (c) G'' versus strain amplitude for the optimized sample and sample type 15.

Table VII shows the ANOVA results for the effect of the temperature on tan δ. The iron sand content and magnetic field both showed a significant influence on tan δ with a confidence level of 99%. It was also apparent that the particle size had much less influence, with a less than 10% contribution.

Finally, an experiment was carried out to compare the value of tan δ for the optimized sample (30-phr iron sand content, 32–45-μm particle size, and 1000-mT magnetic field) with those achieved previously for the sample with the highest value of tan δ in the transition zone (sample type 17). In addition, the unfilled natural rubber was included for comparison (see Figure 9). The values of tan δ for the optimized sample, sample type 17, and unfilled natural rubber were 1.280, 1.216, and 0.803, respectively. As also shown, the tan δ peak of natural rubber was higher compared to those of the optimized sample and sample type 17. However, the widths of the tan δ peaks for the optimized sample and sample type 17 were wider, and tan δ for the optimized sample at $-35°C$ was the highest. This could again be explained as being due to the confinement of molecular chain movement. Because rubber materials are always in practice used in the rubbery phase, the performance and behaviour of the materials in the temperature range after the transition region were more crucial. In the rubbery phase (occurring

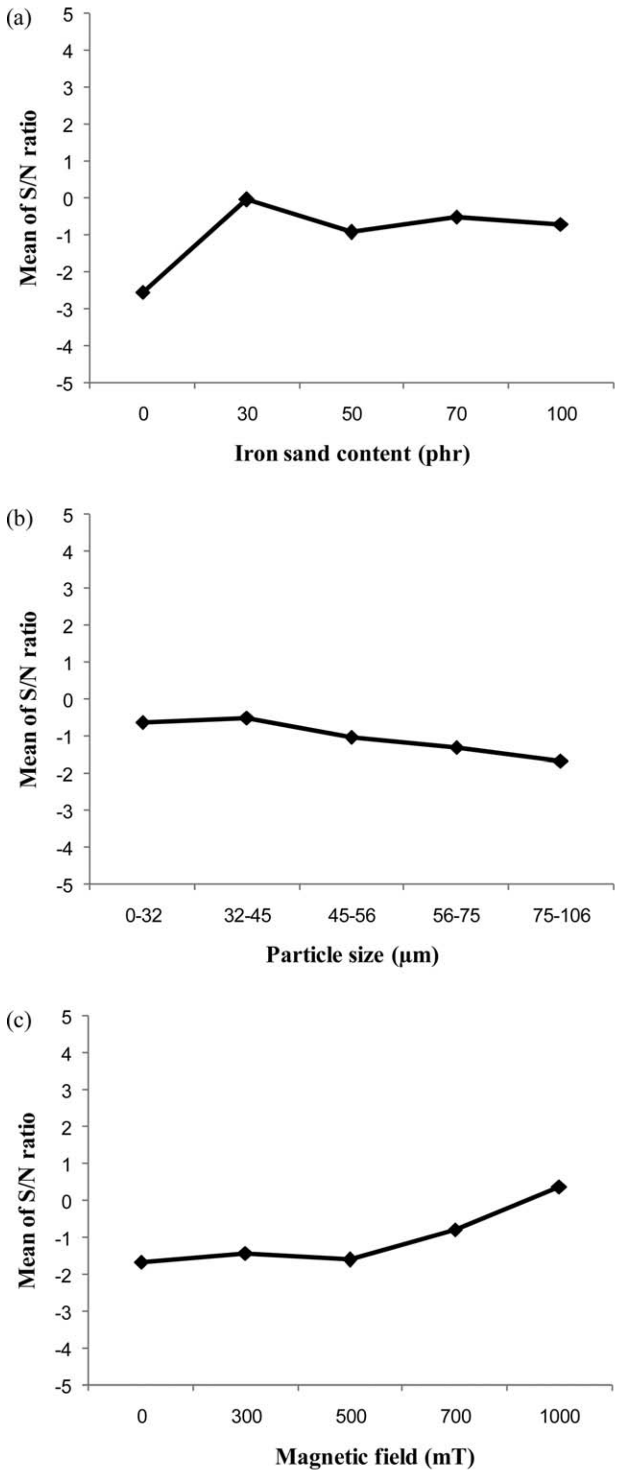

Figure 8. Main effect plots for *S*/*N* of tan δ at $-35°C$: (a) effect of the iron sand content, (b) effect of the iron sand particle size, and (c) effect of the magnetic field during curing.

in the plateau after the peak), it can also be seen that the optimized sample had the largest value of tan δ, followed by sample type 17 and the unfilled natural rubber. This was because, at higher temperatures, the thermal energy was comparable to the potential energy barriers for the viscous flow; therefore, the interfacial friction, breakdown, and reformation of the filler–filler interaction and filler–rubber detachment were the main causes of damping.

Hysteresis

The main effect plots of the *S*/*N*s for hysteresis loss are presented in Figure 10. The relationship between the iron sand content and *S*/*N* was approximately linear, with the amount of energy dissipated increasing with the iron sand content up to 100 phr. The increase in energy dissipated could be attributed to interfacial friction, the breakdown of filler aggregates to release trapped rubber to allow more viscous flow, and filler–rubber detachment and reformation. As shown in Figure 10(b,c), the particle size and magnetic field had minimal influence on the hysteresis loss, but the *S*/*N*s at 45–56 µm and 1000 mT were the highest. It is also noted that the suggested optimum conditions to obtain highest the hysteresis loss were similar to those for the optimum conditions when assessing the influence of the frequency on tan δ. The Taguchi method suggested that the highest hysteresis loss and tan δ could be obtained with high iron sand contents (100 and 70 phr, respectively), with particle size not being greatly influential (although a particle size of 45–56 µm gave the highest values for both hysteresis and tan δ). However, the suggested magnetic field during curing gave a contrary conclusion (1000 and 300 mT, respectively, for hysteresis and tan δ); this could have been due to the different mode of loading during testing (tensile vs shear). This suggested that the energy absorption due to interactions between magnetic particle alignment was less efficient in the tensile mode compared with those in the shear mode with DMA; this was not surprising, given that in tension, it is largely only the spacing increasing between chains, whereas in shear, the spacing within chain between the particles increases (see Figure 11).

Table VIII shows the ANOVA results for the hysteresis loss. The confidence levels for all factors were 98% and higher. From the levels of contribution, it can be seen that the most influential factor by far was the iron sand content; this was followed by the particle size (80.71 and 14.38%, respectively). The influence of the magnetic field was much less at 4.91%.

Figure 12 shows the stress–strain loops of the sample at the suggested optimum conditions (100-phr iron sand, 45–56-µm particle size, and 1000 mT), and those for the highest hysteresis loss achieved previously (sample type 23) after a complete reversed stress cycle. As shown, the area of the hysteresis loop for the optimized sample was larger than that in sample type 23. The amounts of energy lost for the optimized sample and sample type 23 were 160.96 and 154.61 kJ/m^3, respectively. This supported the optimum conditions suggested by the *S*/*N* and ANOVA. As the strain increased, the curvilinear part at the beginning of stretching was attributed to interfacial friction, the breakdown of filler aggregates, and filler–rubber detachment and reformation, and as the strain increased, the amount of energy dissipated increased. This was believed to be mainly dominated by the viscous flow in the rubber phase, as reported in the literature.[35] As the strain increased, the cross-sectional area of the tested samples decreased, and the rubber molecular chains came closer to each other. Under further strain, the

Table VII. ANOVA Results for the Effects of the Temperature on Tan δ

Factor	SS	Degrees of freedom	Confidence level (%)	Contribution (%)
Iron sand content (phr)	0.185	4	99	48.15
Particle size (μm)	0.035	4	70	9.22
Magnetic field (mT)	0.164	4	99	42.62

chains constrained each other; therefore, they slid with respect to each other, and this resulted in a further increase in dissipated energy. When the load was removed, the rubber molecular chains did not completely regain their original configuration, and the energy dissipated was expected to be converted into heat.[35,40]

CONCLUSIONS

In this study, iron sand and natural rubber MREs were manufactured, and experiments were designed with the Taguchi method to assess the effects of the iron sand content, iron sand particle size, and applied magnetic field during curing on the tan δ (over a wide range of frequency, strain amplitude, and temperature) and energy dissipated during cyclic loading. SEM micrographs revealed that the isotropic MREs had homogeneous iron sand particle distribution, and curing the materials under an applied magnetic field at an elevated temperature resulted in the iron sand particles organizing into chainlike columnar structures. For the effect of the frequency on tan δ, the Taguchi method suggested that the optimum conditions were obtained with 70-phr iron sand, a 45–56-μm particle size, and a 300-mT magnetic field; this was supported by the experiment. It was found that the iron sand had the greatest influence on tan δ followed by the particle size and magnetic field. The suggested optimum conditions to obtain the highest hysteresis loss were similar to the optimum conditions suggested when assessing the influence of the frequency on tan δ. The Taguchi method suggested that the highest hysteresis loss could be obtained with a 100-phr iron sand content (slightly different than the 70-phr iron sand content suggested for frequency), with the particle size not being greatly influential (although a particle size of 45–56 μm gave the highest values for both

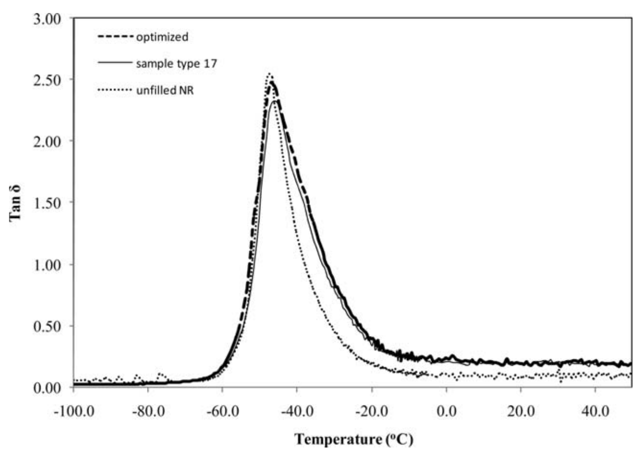

Figure 9. Tan δ versus the temperature for natural rubber (NR), the optimized sample, and sample 17.

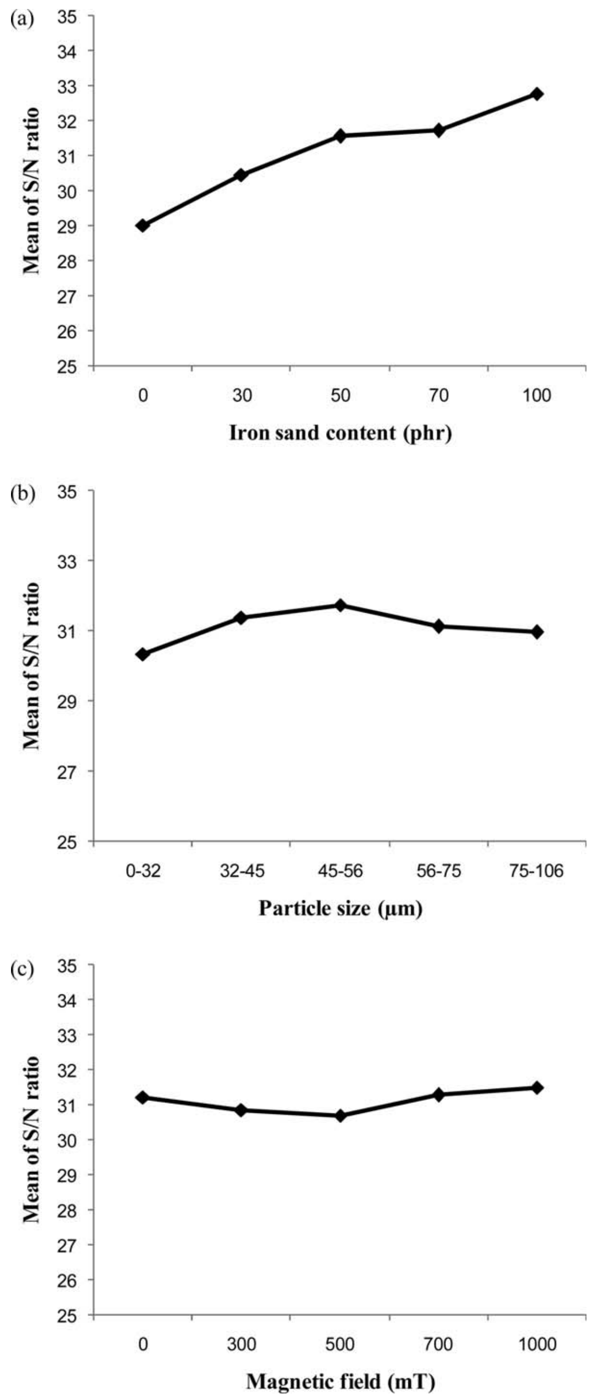

Figure 10. Main effect plots for S/N of hysteresis loss: (a) effect of the iron sand content, (b) effect of the iron sand particle size, and (c) effect of the magnetic field during curing.

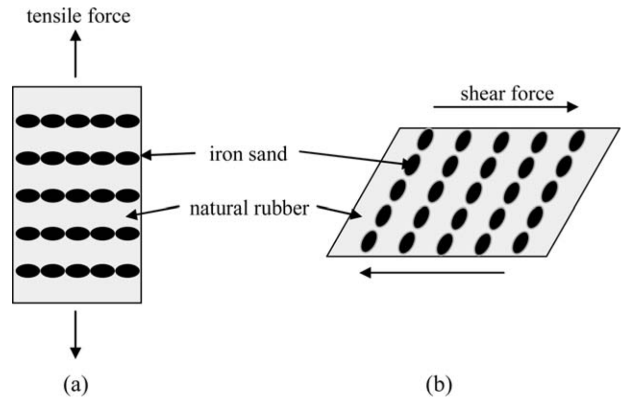

Figure 11. Comparison of the influence of the loading types on the particle separation, (a) tensile and (b) shear modes.

Table VIII. ANOVA Results for the Hysteresis Loss

Factor	SS	Degrees of freedom	Confidence level (%)	Contribution (%)
Iron sand content (phr)	43,038.6	4	99.9	80.71
Particle size (μm)	7669.1	4	99.9	14.38
Magnetic field (mT)	2616.7	4	98	4.91

hysteresis and tan δ). However, the optimum magnetic field during curing was different for the maximization of tan δ and hysteresis loss (300 and 1000 mT, respectively); this could have been due to the different modes of loading during testing (tensile vs shear). For the effect of the strain amplitude on tan δ, none of the factors showed a significant influence on tan δ over a range of strain amplitude; this was attributed to the poor bonding between the iron sand and rubber such that the weak interactions between the iron sand and natural rubber were fully disrupted at low strain amplitudes. Therefore, at high strain amplitudes, the damping was dominated by the viscous flow of the rubber matrix. For

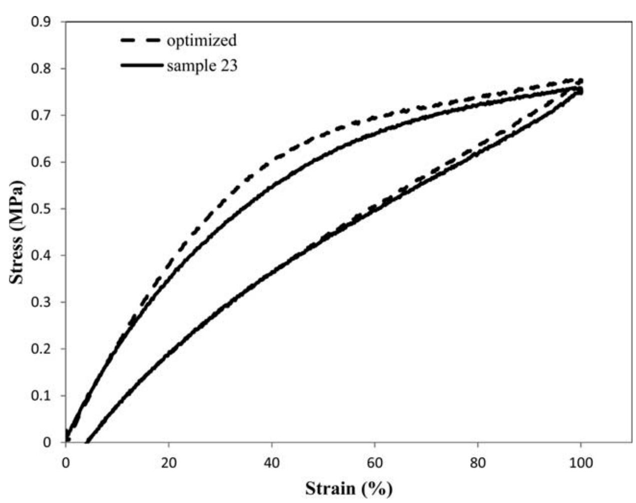

Figure 12. Hysteresis loops of the optimized sample and sample 23.

the effect of the temperature on tan δ, the optimum conditions suggested by the Taguchi method were 30-phr iron sand, a 32–45-μm particle size, and a 1000-mT magnetic field. It was found that addition of iron sand and the formation of magnetic particle chains constrained the conformational changes of the rubber molecular chains from taking part in the relaxation process and, therefore, increased the temperature at which the molecular chains started to mobilize, such that the width of the peak of tan δ increased. The different optimum conditions for different tests carried out herein would appear to have been due to the relatively different amounts of energy absorbed by different degrees that different mechanisms were involved with different loading conditions and at different frequencies and strain amplitudes.

ACKNOWLEDGMENTS

The authors are grateful for the support from the Polymer and Composite Research Group of the University of Waikato.

REFERENCES

1. Lakes, R. S. *J. Compos. Mater.* **2001**, *36*, 287.
2. Jerzy, K.; Daniel, L.; Rafal, M.; Piotr, Z. Smart Magnetic Composites (SMC); Metal, Ceramic and Polymeric Composites for Various Uses; InTech: Rijeka, Croatia, **2011**.
3. Chokkalingam, R.; Rajasabai Senthur, P.; Mahendran, M. *J. Compos. Mater.* **2010**, *45*, 1545.
4. Jerzy, K.; Michal, K.; Daniel, L. *Smart Mater. Struct.* **2011**, *20*, 12.
5. Chen, L.; Gong, X. L.; Li, W. H. *Polym. Test.* **2008**, *27*, 340.
6. Fuchs, A.; Zhang, Q.; Elkins, J.; Gordaninejad, F.; Evrensel, C. *J. Appl. Polym. Sci.* **2007**, *105*, 2497.
7. Ginder, J. *Proc. SPIE* **1999**, *3675*, 131.
8. Lerner, A. A.; Cunefare, K. A. *J. Intell. Mater. Syst. Struct.* **2008**, *19*, 551.
9. Sun, T. L.; Gong, X. L.; Jiang, W. Q.; Li, J. F.; Xu, Z. B.; Li, W. H. *Polym. Test.* **2008**, *27*, 520.
10. Wang, Y.; Hu, Y.; Deng, H.; Gong, X.; Zhang, P.; Jiang, W.; Chen, Z. *Polym. Eng. Sci.* **2006**, *46*, 264.
11. Lokander, M.; Stenberg, B. *Polym. Test.* **2003**, *22*, 677.
12. Lokander, M.; Stenberg, B. *Polym. Test.* **2003**, *22*, 245.
13. Carlson, J. D.; Jolly, M. R. *Mechatronics* **2000**, *10*, 555.
14. Blom, P.; Kari, L. *Polym. Test.* **2005**, *24*, 656.
15. Chen, L.; Gong, X.-L.; Jiang, W.-Q.; Yao, J.-J.; Deng, H.-X.; Li, W.-H. *J. Mater. Sci.* **2007**, *42*, 5483.
16. Alberdi-Muniain, A.; Gil-Negrete, N.; Kari, L. *Plast. Rubber Compos.* **2012**, *41*, 310.
17. Sun, Y.; Zhou, X.; Liu, Y.; Zhao, G.; Jiang, Y. *Mater. Res. Bull.* **2009**, *45*, 878.
18. Makled, M. H.; Matsui, T.; Tsuda, H.; Mabuchi, H.; El-Mansy, M. K.; Morii, K. *J. Mater. Process. Technol.* **2005**, *160*, 229.
19. Dobrzanski, L. A.; Tomiczek, A.; Tomiczek, B.; Slawska, A.; Iesenchuk, O. *J. Achievements Mater. Manufacturing Eng.* **2009**, *37*, 16.

20. Bryan, K. R.; Robinson, A.; Briggs, R. M. *Marine Geol.* **2007**, *236*, 45.
21. Briggs, R. M.; Laurent, J. C.; Hume, T. M.; Swales, A. In AusIMM New Zealand Branch Annual Conference, New Zealand; AusIMM: Carlton South Vic., Australia, **2009**, p 41.
22. Montgomery, D. C. Design and Analysis of Experiments; Wiley: Hoboken, NJ, **1997**.
23. Arvidsson, M.; Gremyr, I. In Robust Design Methodology for Reliability; Wiley: Hoboken, NJ, **2009**.
24. Mitra, A. Wiley Interdiscip. *Rev. Comput. Stat.* **2011**, *3*, 472.
25. Derakhshandeh, B.; Shojaei, A.; Faghihi, M. *J. Appl. Polym. Sci.* **2008**, *108*, 3808.
26. Bhattacharya, M.; Bhowmick, A. K. *Wear* **2010**, *269*, 152.
27. Roy, R. K. Design of Experiments Using the Taguchi Approach: 16 Steps to Product and Process Improvement; Wiley: New York, **2001**.
28. Khimi, S. R.; Pickering, K. L. *J. Appl. Polym. Sci.* **2013**, *131*, 40008.
29. Boczkowska, A.; Awietjan, S. F.; Pietrzko, S. A.; KurzydÅowski, K. *J. Compos. B* **2012**, *43*, 636.
30. Kari, L.; Blom, P. *Plast. Rubber Compos.* **2005**, *34*, 365.
31. Shirazi, M.; Talma, A. G.; Noordermeer, J. W. M. *J. Appl. Polym. Sci.* **2013**, *128*, 2255.
32. Han, J.; Shi, N.; Xie, L.; Ma, Y.; Wu, C. *J. Macromol. Sci. B Phys.* **2010**, *49*, 429.
33. Liu, Q. X.; Ding, X. B.; Zhang, H. P.; Yan, X. *J. Appl. Polym. Sci.* **2009**, *114*, 2655.
34. Kar, K. K.; Bhowmick, A. K. *Polym. Eng. Sci.* **1998**, *38*, 1927.
35. Kucherskii, A. M. *Polym. Test.* **2005**, *24*, 733.
36. Arrighi, V.; McEwen, I. J.; Qian, H.; Serrano Prieto, M. B. *Polymer* **2003**, *44*, 6259.
37. Yanceng, F.; Xinglong, G.; Shouhu, X.; Wei, Z.; Jian, Z.; Wanquan, J. *Smart Mater. Struct.* **2011**, *20*, 1.
38. Hathaway, K.; Clark, A.; Teter, J. *Metall. Mater. Trans. A* **1995**, *26*, 2797.
39. Rendek, M.; Lion, A. *Int. J. Solids Struct.* **2010**, *47*, 2918.
40. Ahankari, S. S.; Kar, K. K. *Polym. Eng. Sci.* **2010**, *50*, 871.